

## Article

# Detecting the Spatiotemporal Variation of Vegetation Phenology in Northeastern China Based on MODIS NDVI and Solar-Induced Chlorophyll Fluorescence Dataset

Ruixin Zhang<sup>1</sup>, Yuke Zhou<sup>2,\*</sup> , Tianyang Hu<sup>3,\*</sup>, Wenbin Sun<sup>1</sup>, Shuhui Zhang<sup>4</sup>, Jiawei Wu<sup>2</sup> and Han Wang<sup>2</sup>

<sup>1</sup> College of Geoscience and Surveying Engineering, China University of Mining and Technology, Beijing 100083, China

<sup>2</sup> Key Laboratory of Ecosystem Network Observation and Modeling, Institute of Geographic and Nature Resources Research, Chinese Academy of Sciences, Beijing 100101, China

<sup>3</sup> State Environmental Protection Key Laboratory of Quality Control in Environmental Monitoring, China National Environmental Monitoring Centre, Beijing 100012, China

<sup>4</sup> State Key Laboratory of Herbage Improvement and Grassland Agro-Ecosystems, College of Pastoral Agriculture Science and Technology, Lanzhou University, Lanzhou 730020, China

\* Correspondence: zhoyuk@igsrr.ac.cn (Y.Z.); huty@cnemc.cn (T.H.)

**Abstract:** Vegetation phenology is a crucial biological indicator for monitoring changes in terrestrial ecosystems and global climate. Currently, there are limitations in using traditional vegetation indices for phenology monitoring (e.g., greenness saturation in high-density vegetation areas). Solar-induced chlorophyll fluorescence (SIF), a novel remote sensing product, has great potential in depicting seasonal vegetation dynamics across various regions with different vegetation covers and latitudes. In this study, based on the GOSIF and MODIS NDVI data from 2001 to 2020, we extracted vegetation phenological parameters in Northeastern China by using Double Logistic (D-L) fitting function and the dynamic threshold method. Then, we analyzed the discrepancy in phenological period and temporal trend derived from SIF and NDVI data at multiple spatiotemporal scales. Furthermore, we explored the response of vegetation phenology to climate change and the persistence of phenological trends (Hurst exponent) in Northeastern China. Generally, there is a significant difference in trends between SIF and NDVI, but with similar spatial patterns of phenology. However, the dates of key phenological parameters are distinct based on SIF and MODIS NDVI data. Specifically, the start of season (SOS) of SIF started later (about 10 days), and the end of season (EOS) ended earlier (about 36 days on average). In contrast, the fall attenuation of SIF showed a lag process compared to NDVI. This implies that the actual period of photosynthesis, that is, length of season (LOS), was shorter (by 46 days on average) than the greenness index. The position of peak (POP) is almost the same between them. The great difference in results from SIF and NDVI products indicated that the vegetation indexes seem to overestimate the time of vegetation photosynthesis in Northeastern China. The Hurst exponent identified that the future trend of SOS, EOS, and POP is dominated by weak inverse sustainability, indicating that the future trend may be opposite to the past. The future trend of  $LOS_{SIF}$  and  $LOS_{NDVI}$  are opposite; the former is dominated by weak inverse sustainability, and the latter is mainly weak positive sustainability. In addition, we speculate that the difference between SIF and NDVI phenology is closely related to their different responses to climate. The vegetation phenology estimated by SIF is mainly controlled by temperature, while NDVI is mainly controlled by precipitation and relative humidity. Different phenological periods based on SIF and NDVI showed inconsistent responses to pre-season climate. This may be the cause of the difference in the phenology of SIF and NDVI extraction. Our results imply that canopy structure-based vegetation indices overestimate the photosynthetic cycle, and the SIF product can better track the phenological changes. We conclude that the two data products provide a reference for monitoring the phenology of photosynthesis and vegetation greenness, and the results also have a certain significance for the response of plants to climate change.



check for updates

**Citation:** Zhang, R.; Zhou, Y.; Hu, T.; Sun, W.; Zhang, S.; Wu, J.; Wang, H. Detecting the Spatiotemporal Variation of Vegetation Phenology in Northeastern China Based on MODIS NDVI and Solar-Induced Chlorophyll Fluorescence Dataset. *Sustainability* **2023**, *15*, 6012. <https://doi.org/10.3390/su15076012>

Academic Editors: Xinchang Zhang, Yongjian Ruan and Ying Sun

Received: 21 January 2023

Revised: 22 March 2023

Accepted: 29 March 2023

Published: 30 March 2023



**Copyright:** © 2023 by the authors. Licensee MDPI, Basel, Switzerland. This article is an open access article distributed under the terms and conditions of the Creative Commons Attribution (CC BY) license (<https://creativecommons.org/licenses/by/4.0/>).

**Keywords:** vegetation phenology; NDVI; solar-induced chlorophyll fluorescence; climate change; vegetation phenology; Northeastern China

---

## 1. Introduction

Vegetation phenology refers to the periodic phenomena such as germination, leaf spreading, flowering, and defoliation of vegetation in the process of growth influenced by climate and other driving factors [1], which can reflect the interaction of vegetation phenological parameters in the abiotic environment [2,3]. By controlling seasonal changes in vegetation and physiological functions such as photosynthesis, changes in vegetation phenology can affect the structure and function of ecosystems [4]. The change in vegetation phenology affects the structure and function of ecosystems and climate change. Therefore, it is crucial to monitor vegetation phenology changes, due to the variety of vegetation types, high plant coverage, and sensitivity to climate change in Northeastern China. Thus, the study of vegetation phenology in this region is of great significance for understanding the response of phenology to climate change.

Satellite remote sensing data can provide effective information on vegetation phenology at multiple scales, and have become an outstanding tool for monitoring surface phenology. Traditional vegetation indices [5,6], such as the Normalized Difference Vegetation Index (NDVI), Enhanced Vegetation Index (EVI), and Leaf Area Index (LAI), are widely used in vegetation phenology research [7,8]. However, vegetation indices have some uncertainties in characterizing vegetation phenology. On the one hand, it is difficult to accurately capture the greenness of the vegetation canopy due to the influence of snow and bare rock on the vegetation index signal [7,9–11]. On the other hand, the vegetation index is usually related to the morphological characteristics of the vegetation canopy. There is an inconsistency between the morphological characteristics of the vegetation canopy and the physiological characteristics of the vegetation, which results in the accuracy of phenology analysis based on the morphological changes in the vegetation canopy [12–14].

As a complement to the vegetation index, Solar-induced chlorophyll fluorescence (SIF) offers new possibilities for monitoring vegetation function spatially. SIF is the spectral signals emitted by vegetation under light conditions through photosynthesis at wavelengths of 650–800 nm in the red band (around 690 nm). There are two peaks in the near-infrared band (around 740 nm), and the data are insensitive to both atmospheric and cloud scattering, which can directly reflect the dynamic changes in the photosynthesis of vegetation. Thus, SIF has a stronger physiological basis compared with traditional vegetation indices. With the continuous development of observation satellites such as GOSAT, GOME-2, and OCO-2, it is possible to invert SIF and monitor vegetation phenology studies on a global scale. However, the current studies based on SIF mainly focus on the consistency analysis between SIF and Gross Primary Productivity (GPP) and the comparison of SIF with other indicators [15,16], rather than the calculation of vegetation phenology values using SIF. In addition, previous studies [17] have been conducted mainly on a global scale and in larger study areas. The relationship between SIF and vegetation indices changes with the change in spatial resolution and the increase in global temperature.

Vegetation phenology in the high latitudes of the northern hemisphere shows a trend of earlier rejuvenation and later yellowing in recent years. In addition, the stress of abiotic factors (temperature, precipitation, relative humidity, etc.) leads to a complex spatiotemporal pattern of vegetation phenology. Located in the middle and high latitudes, Northeastern China has high vegetation cover and is highly sensitive to climate change, which is an ideal region for studying vegetation growth and phenological changes. Therefore, this paper uses SIF and NDVI data to estimate the vegetation phenology in Northeastern China from 2001 to 2020, and focuses on the following issues: (1) the spatiotemporal distribution of vegetation phenology in the context of climate change; (2) the change patterns of different vegetation types; and (3) the main driving forces of different vegetation phenology changes.

This paper has a positive significance in monitoring the potential of vegetation for photosynthetic phenology and exploring the environmental impact mechanism of vegetation phenology through SIF.

## 2. Materials and Methods

### 2.1. Study Area

The study region is located in Northeastern China ( $115^{\circ}05' \sim 135^{\circ}09' \text{ E}$ ,  $38^{\circ}40' \sim 53^{\circ}34' \text{ N}$ ), the topography of the region is complex, and the administrative divisions include the provinces of Heilongjiang, Jilin, and Liaoning, as well as the central-eastern part of Inner Mongolia. This area belongs to the temperate continental monsoon climate, with warm and rainy summers and cold and dry winters [18]. According to the spatial differences of topography and hydrothermal conditions, the vegetation types in the region [19] are mainly divided into the following eight types (Figure 1): cultivated vegetation (central and eastern Sanjiang plains), scrub, grassland (sporadically distributed in the southwest), steppe (Hulunbuir and southern Daxinganling), meadow (central-eastern part), coniferous forest (northern Daxinganling), broad-leaved forest (Xiaoxinganling and Changbai Mountain), and mixed coniferous and broad-leaved forest (sporadically distributed in Xiaoxinganling and Changbai Mountain).

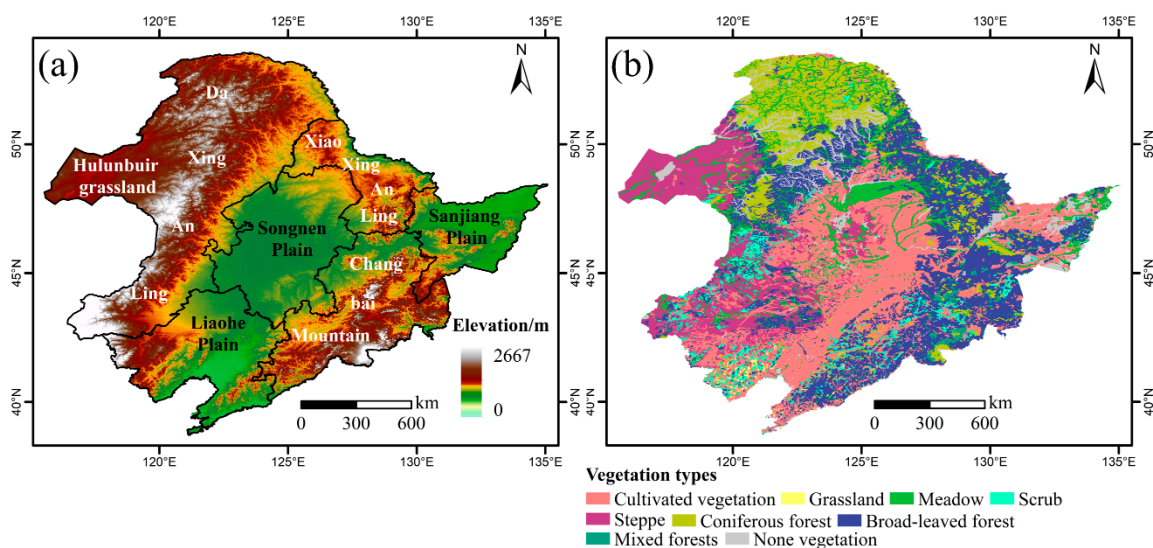


**Figure 1.** Maps of topographic (a) and vegetation types (b) in Northeastern China.

### 2.2. Data Sources and Reprocessing

#### 2.2.1. SIF Datasets

The SIF data used in this study are a long time series dataset for 2001–2020 [20] Global “OCO-2” SIF (GOSIF) (<http://globalecology.unh.edu>, accessed on 1 September 2022), with a temporal resolution of 8 d and a spatial resolution of  $0.05^{\circ}$ . Solar-induced chlorophyll fluorescence is mainly through discrete OCO2-SIF data, MODIS surface reflection data, and meteorological reanalysis data in a data-driven model calculation [21,22]. It is better than traditional vegetation indices in characterizing the vegetation dynamics of surface ecosystems.

#### 2.2.2. NDVI Datasets

The MODIS data (MOD13Q1) used in this study are derived from the longtime series vegetation index dataset from 2001 to 2020 provided by the LAADS DAAC data center (<https://search.earthdata.nasa.gov>, accessed on 1 September 2022), with a temporal resolution of 16 d and a spatial resolution of 250 m. The data contained noise due to environmental conditions, sensor accuracy, etc. Therefore, the NDVI data are processed by de-clouding, aerosol, and masking. Finally, the time series NDVI dataset is generated.

### 2.2.3. Meteorological Data

Meteorological data from 2001 to 2020 were used to analyze the effects of climate factors on vegetation phenology in Northeastern China, including temperature (Temp), precipitation (Prcp), and relative humidity (RH). The temperature and precipitation data for the monthly precipitation dataset and mean air temperature datasets are from the monthly precipitation dataset and the average temperature dataset provided by the National Tibetan Plateau Scientific Data Center [23–25] (<http://data.tpdc.ac.cn/>, accessed on 1 September 2022). This dataset [26] is generated by the Delta spatial downscaling scheme in China, based on the global 0.5° climate dataset published by Climatic Research Unit (CRU) and the global high-resolution climate dataset published by WorldClim. Additionally, it uses 496 independent weather observation point data for validation, whose results are credible. The relative humidity data were obtained from the monthly average relative humidity of 1 km provided by the National Science Center (<http://www.geodata.cn/>, accessed on 1 September 2022), a national platform for basic conditions of science and technology.

### 2.2.4. Data of Vegetation and Topography

Vegetation data are from the Vegetation Map of the People's Republic of China (1:1,000,000) [19] (<http://www.resdc.cn/data.aspx?daTaId=122>, accessed on 1 September 2022). The vegetation classification criteria based on the vegetation community appearance, dominant species composition, and ecogeographical characteristics are adopted in accordance with the characteristics of the Chinese class distribution of the vegetation and the ecological geography, which provides important basic work for ecology and geography research and guiding ecological construction.

Geographic Digital Elevation Model (Digital Elevation Model, DEM) is derived from ASTER GDEM V2 version of digital elevation data product with spatial resolution of 30 m, provided by Geospatial Data Cloud site, Computer Network Information Center, Chinese Academy of Sciences (<http://www.gscloud.cn/>, accessed on 1 September 2022).

## 2.3. Research Methods

### 2.3.1. Phenology Extraction

The SIF time series with noise and outliers removed can be used to invert the vegetation phenology with higher accuracy and more reliable results. Based on the Double Logistic (D-L) fitting method [27], we fit the SIF time series curves from 2001 to 2020 in Northeastern China (Figure 2). Combined with the curve fitting characteristics, the vegetation regreening period was set at 10% on the left side of the curve [28–30], and the withered period was set at 50% on the right side. The dynamic [31] threshold method was used to extract vegetation phenology in Northeastern China. The start of season (SOS), end of season (EOS), length of season (LOS), and position of peak (POP) were selected as the discriminant parameters of vegetation phenology in the study area.

### 2.3.2. Trend Analysis

Simple linear regression is used to analyze the temporal trends of vegetation phenology parameters in Northeastern China, calculated as follows:

$$\text{Slope} = \frac{\sum_{i=1}^n (i \times Y_i) - \sum_{i=1}^n i \sum_{i=1}^n Y_i}{n \sum_{i=1}^n i^2 - (\sum_{i=1}^n i)^2} \quad (1)$$

where  $i$  denotes the year,  $n$  denotes the number of samples ( $n=20$ ), and  $Y_i$  denotes the vegetation phenology parameter values for the year  $i$ . If  $\text{Slope} < 0$ , there is an advance (shortening) trend, abbreviated as AT; if  $\text{Slope} > 0$ , there is a delayed (increasing) trend, abbreviated as DT.

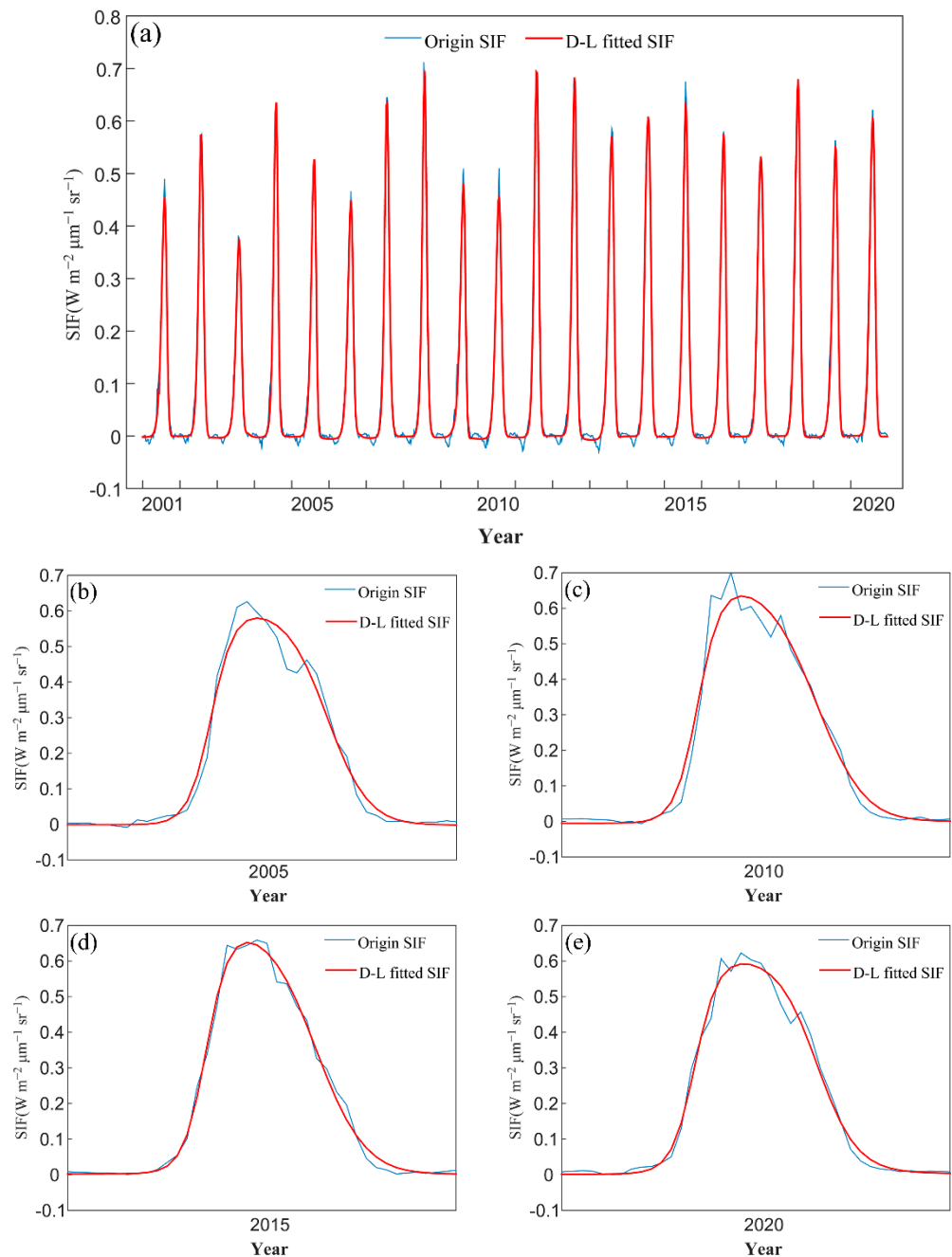


**Figure 2.** Double Logistic (D-L) filtering of SIF time series in Northeastern China during 2001–2020 (a); D-L filtering of SIF time series in 2005 (b); D-L filtering of SIF time series in 2010 (c); D-L filtering of SIF time series in 2015 (d); D-L filtering of SIF time series in 2020 (e).

### 2.3.3. Persistence Analysis

Hurst Index (H) [32] is one of the main methods for quantitative description of long-range dependence, which is widely used in hydrology, climate, earthquakes, and geology. Later, it was gradually applied to remote sensing and vegetation [33–36]. In this study, R/S analysis method was adopted to calculate the change trend of vegetation phenology in Northeastern China by pixel to reflect the persistence of the change trend. The value range of H is between [0 and 1], and the strength of vegetation phenology persistence can be judged by the size of the H value. The value of H is generally divided into three forms:

- (1) When  $0.5 < H < 1$ , which indicates that the time series is sustainable or persistent with the past long-term change; the greater the H value, the stronger the sustainability or persistence;
- (2) When  $H = 0.5$ , which indicates that the time series is random and long-term correlation does not exist;
- (3) When  $0 < H < 0.5$ , which indicates that time series has anti-sustainability or opposite direction with the past long-term change; the smaller the H value, the stronger the anti-sustainability.

On this basis, the H value of vegetation phenological time series in Northeastern China is divided into four types: strong anti-sustainability ( $0.15 \leq H < 0.35$ ), abbreviated as SAS; weak anti-sustainability ( $0.35 \leq H < 0.5$ ), abbreviated as WAS; weak sustainability ( $0.5 < H < 0.75$ ), abbreviated WS; strong sustainability ( $H \geq 0.75$ ), abbreviated SS.

The change trend of vegetation phenological parameters and sustainability results were superimposed to obtain the change trend–sustainability results shown in Table 1.

**Table 1.** Classification of future trends of vegetation phenology in Northeastern China.

Trend/Sustainability	SAS	WAS	WS	SS
AT	AT-SAS	AT-WAS	AT-WS	AT-SS
DT	DT-SAS	DT-WAS	DT-WS	DT-SS

#### 2.3.4. Correlation Analysis

The degree of correlation between variables is usually expressed by the correlation coefficient R. In this paper, Spearman's correlation coefficient was used to study the correlation between vegetation phenology parameters and meteorological factors (Temp, Prcp, and RH) at pixel scale, calculated as follows:

$$R_{XY} = \frac{Cov(X, Y)}{\sqrt{D(X)}\sqrt{D(Y)}} \quad (2)$$

where  $Cov(X, Y)$  denotes the covariance between the variable X and Y, and  $D(X)$  and  $D(Y)$  denote the variance for X and Y

The range of values for R is  $[-1, 1]$ . If  $R > 0$ , there is a positive correlation between variables; that is, one variable increases as the other increases. If  $R < 0$ , it means that the two are negatively correlated.

### 3. Results

#### 3.1. Spatial Distribution of Vegetation Phenology

We retrieved vegetation phenology parameters from 2001 to 2020 in Northeastern China using SIF and MODIS NDVI, then estimated the multi-annual mean of each pixel for spatial analysis (Figure 3). The results showed that there were significant differences between the phenology results based on SIF and NDVI data. The  $SOS_{SIF}$  mainly concentrated on days 113–170 (Figure 3a), with an area share of 97.9%; the  $SOS_{NDVI}$  mainly concentrated on days 110–157 (Figure 3b), with an area of 93.4%. The  $SOS_{SIF}$  and the  $SOS_{NDVI}$  of the vegetation were higher in the central plain and the eastern Sanjiang plain than in other areas. The  $EOS_{SIF}$  was mainly concentrated on days 240–265 (Figure 3c), with an area of 96.6%, and the  $EOS_{SIF}$  were predated in the coniferous forests in northern Daxinganling and the broad-leaved forests in Xiaoxinganling than in other areas. The  $EOS_{NDVI}$  was primarily focused on days 278–299 (Figure 3d), with an area of 91.3%, and the EOS of Hulunbuir was the latest. The  $LOS_{SIF}$  was mainly concentrated on days 83–149 (Figure 3e), accounting for 96.6% of the total area. The  $LOS_{NDVI}$  was mainly concentrated on days 130–191 (Figure 3f), with an area of 92.4%. They first occurred in Songliao and Sanjiang Plain. The  $POP_{SIF}$  was mainly concentrated on days 190–226 (Figure 3g), accounting for 97.7% of the total area. The  $POP_{NDVI}$  was primarily concentrated on days 202–228 (Figure 3h), accounting

for 94.0% of the total area, with the  $POP_{SIF}$  and the  $POP_{NDVI}$  occurring most recently in southern Daxinganling, Songliao, and Sanjiang plains.

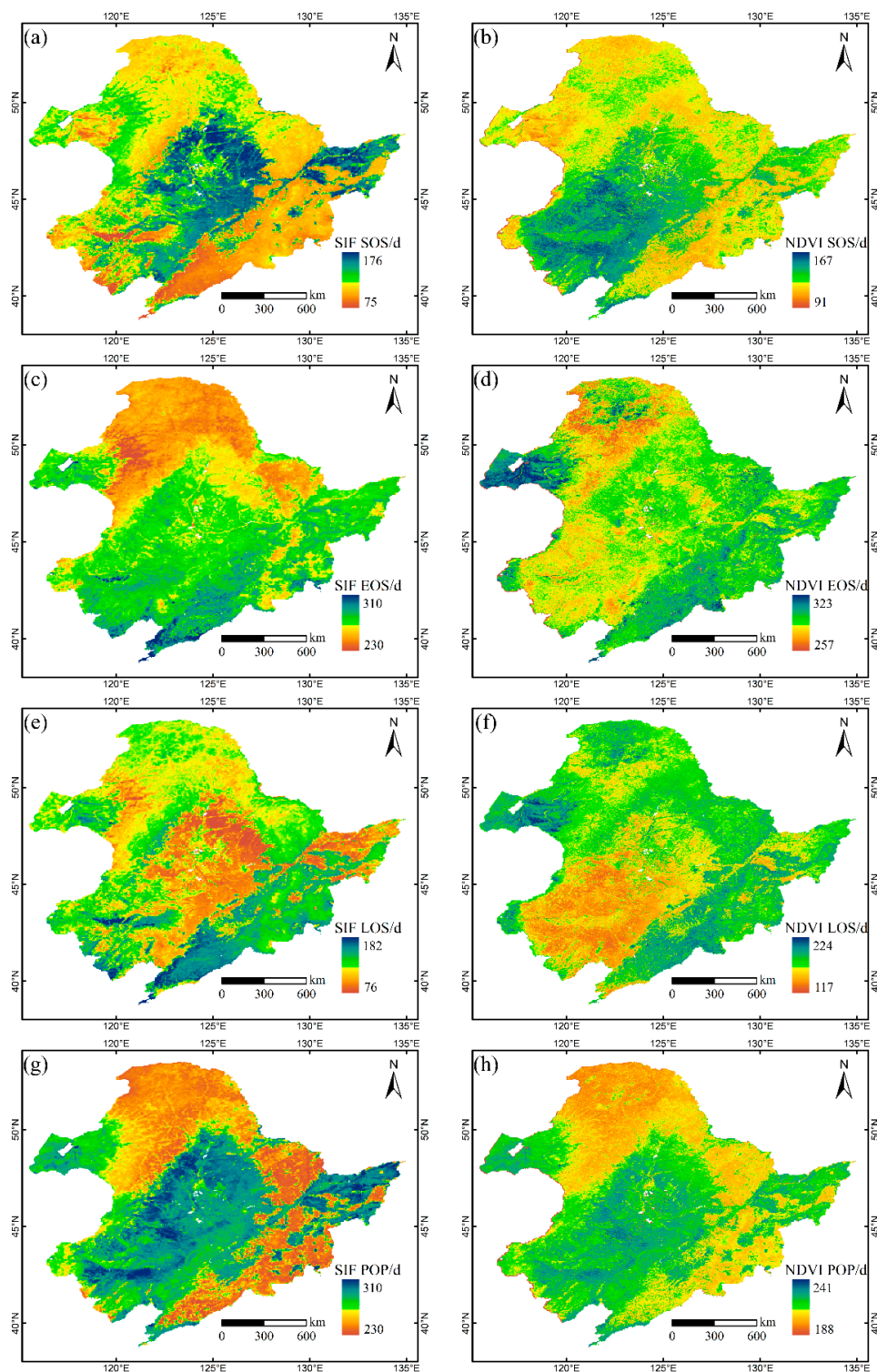


**Figure 3.** Spatial distribution of multi-year mean vegetation phenology based on SIF and NDVI in Northeastern China from 2001 to 2020. (a) SOS (start of season) extracted by SIF( $SOS_{SIF}$ ); (b) SOS extracted by NDVI( $SOS_{NDVI}$ ); (c) EOS (end of season) extracted by SIF( $EOS_{SIF}$ ); (d) EOS extracted by NDVI( $EOS_{NDVI}$ ); (e) LOS extracted by SIF( $LOS_{SIF}$ ); (f) LOS (length of season) extracted by NDVI( $LOS_{NDVI}$ ); (g) POP (position of pop) extracted by SIF( $POP_{SIF}$ ); (h) POP extracted by NDVI( $POP_{NDVI}$ ).

By calculating the average of the phenological indicators in the study area (Table 2). The results showed that the  $SOS_{SIF}$  was closer to the  $SOS_{NDVI}$ , which was about 10 days later than the latter. The mean value of the  $EOS_{SIF}$  predated the  $EOS_{NDVI}$  by about 40 days. The  $LOS_{SIF}$  was generally shorter than the  $LOS_{NDVI}$  because the  $EOS_{SIF}$  was generally more advanced than the  $EOS_{NDVI}$ . The  $POP_{SIF}$  was nearly consistent with the  $POP_{NDVI}$ .

**Table 2.** Average values of the phenological parameters and the change trends based on SIF and NDVI in Northeastern China from 2001 to 2020.

Phenological Parameters	Data Type	Mean Value/d	Change Trend Mean/d
SOS	SIF	138	−0.24
	NDVI	128	2.09
EOS	SIF	254	0.07
	NDVI	290	0.47
LOS	SIF	116	0.30
	NDVI	162	−1.61
POP	SIF	210	−0.13
	NDVI	214	−0.07

The multi-year phenological mean values of different vegetation types in Northeastern China from 2001 to 2020 were analyzed (Figure 4). It can be seen that the  $SOS_{SIF}$  of Grassland (GL) was more advanced than the  $SOS_{NDVI}$ , while the  $SOS_{SIF}$  of other vegetation was later than the  $SOS_{NDVI}$ . Meadow (MD)  $SOS_{SIF}$  and  $SOS_{NDVI}$  had the largest difference, 17 days in advance, while the difference between Scrub (SC)  $SOS_{SIF}$  and  $SOS_{NDVI}$  was the smallest and advanced by only 1 day. The  $EOS_{SIF}$  of all vegetation was earlier than the  $EOS_{NDVI}$ , and the  $LOS_{SIF}$  was shorter than the  $LOS_{NDVI}$ , among which the  $EOS_{SIF}$  of GL was 12 days ahead of the  $EOS_{NDVI}$ , and the  $LOS_{SIF}$  was 20 days shorter than the  $LOS_{NDVI}$ . The  $EOS_{SIF}$  was 43 days ahead of the  $EOS_{NDVI}$  in Conifer broad-leaved mixed forest (Mix B-C), and the  $LOS_{SIF}$  was 50 days ahead. The  $POP_{SIF}$  of all vegetation types was within 10 days ahead of the  $POP_{NDVI}$ , which was more consistent.

### 3.2. Trends in Vegetation Phenology

The trend analysis of vegetation phenology indicators in Northeastern China from 2001 to 2020 (Figure 5). The findings revealed that the trends of the  $SOS_{SIF}$  and the  $SOS_{NDVI}$  in western Hulunbuir, northern Daxinganling, and Changbai Mountain were diametrically opposed, with the former showing a weak delayed trend and the latter showing a weak advanced trend. Both the  $EOS_{SIF}$  and the  $EOS_{NDVI}$  showed a delayed trend in southern Daxinganling and Liaohe Plain. The vegetation  $EOS_{SIF}$  showed an opposite trend to the  $EOS_{NDVI}$  in other areas; the former showed a predated trend, and the latter showed a delayed trend. Advance (delay) of the SOS and delay (advance) of the EOS would lead to prolonging (shortening) of the LOS accordingly. Therefore, the trend of the  $LOS_{SIF}$  and the  $LOS_{NDVI}$  in each region is consistent with that of the EOS. That is, the  $LOS_{SIF}$  and the  $LOS_{NDVI}$  both showed a delayed trend in southern Daxinganling and Liaohe Plain, while the  $LOS_{SIF}$  showed an advanced trend and the  $LOS_{NDVI}$  showed a delayed trend in other regions. The  $POP_{SIF}$  and the  $POP_{NDVI}$  showed a delayed trend in Hulunbeier, southern Daxinganling, and parts of Liaohe Plain, while the  $POP_{SIF}$  showed an early trend and the  $POP_{NDVI}$  showed a weak delayed trend in other regions.

By calculating the average of trends in different phenological indicators in the study area (Table 2), the  $SOS_{SIF}$  had an overall advanced trend, and the trend of the  $SOS_{NDVI}$  was delayed, both of which were contrary. The  $EOS_{SIF}$  and the  $EOS_{NDVI}$  showed a latency trend. However, the delayed trend of the  $EOS_{NDVI}$  was more pronounced. The advancement of the  $SOS_{SIF}$  and the delay of the  $EOS_{SIF}$  led to an overall trend of prolongation of the  $LOS_{SIF}$ . The delayed trend of the  $SOS_{NDVI}$  was much larger than that of the  $EOS_{NDVI}$ , so the total trend of the  $LOS_{NDVI}$  was shortened. The  $POP_{SIF}$  was consistent with the  $POP_{NDVI}$ , and both indicated a weak trend of advance.

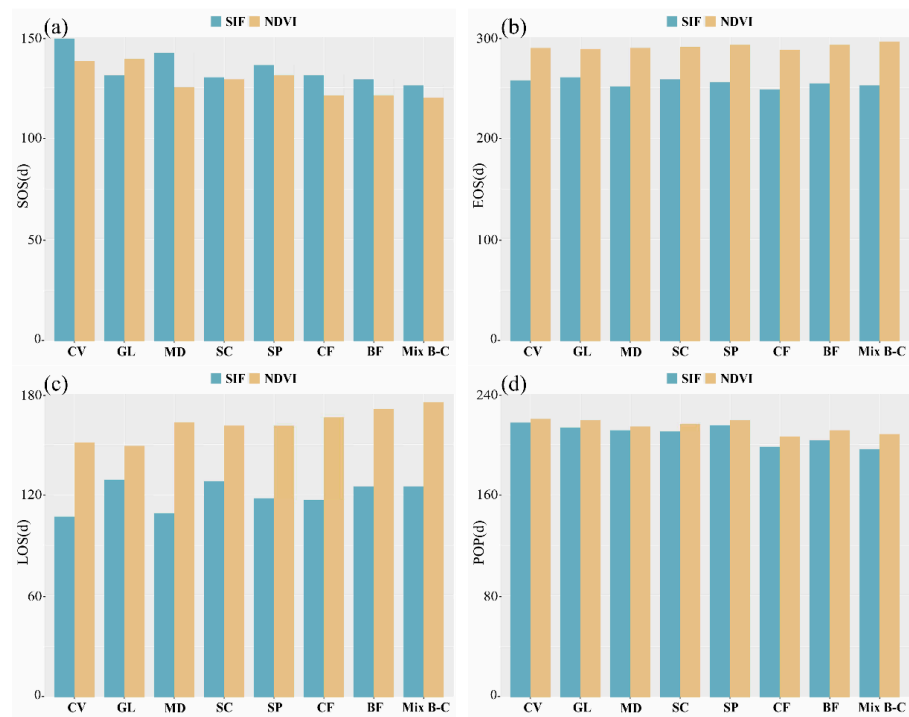


**Figure 4.** Phenology of different vegetation types in Northeastern China from 2001 to 2020. (a) SOS of different vegetation types based on SIF and NDVI; (b) EOS of different vegetation types based on SIF and NDVI; (c) LOS of different vegetation types based on SIF and NDVI; (d) POP of different vegetation types based on SIF and NDVI (CV: cultivated vegetation; GL: grassland; MD: meadow; SC: scrub; SP: steppe; CF: coniferous forest; BF: broad-leaved forest; Mix B-C: conifer-broad leaved mixed forest).

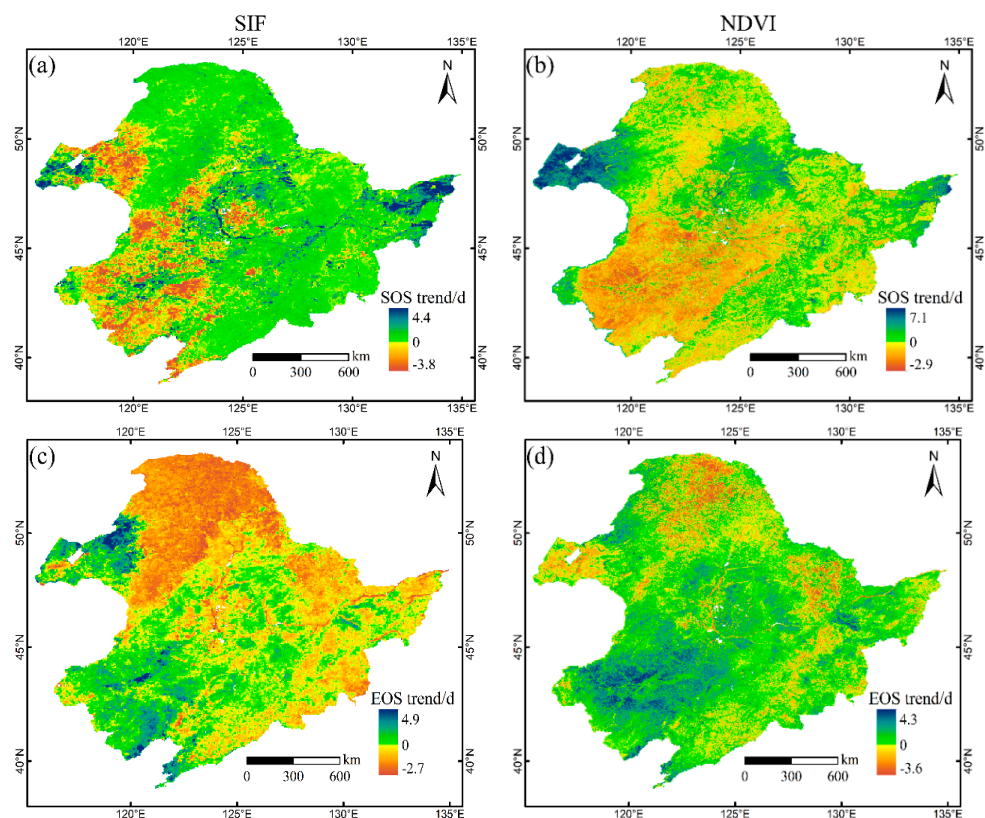


**Figure 5.** Cont.

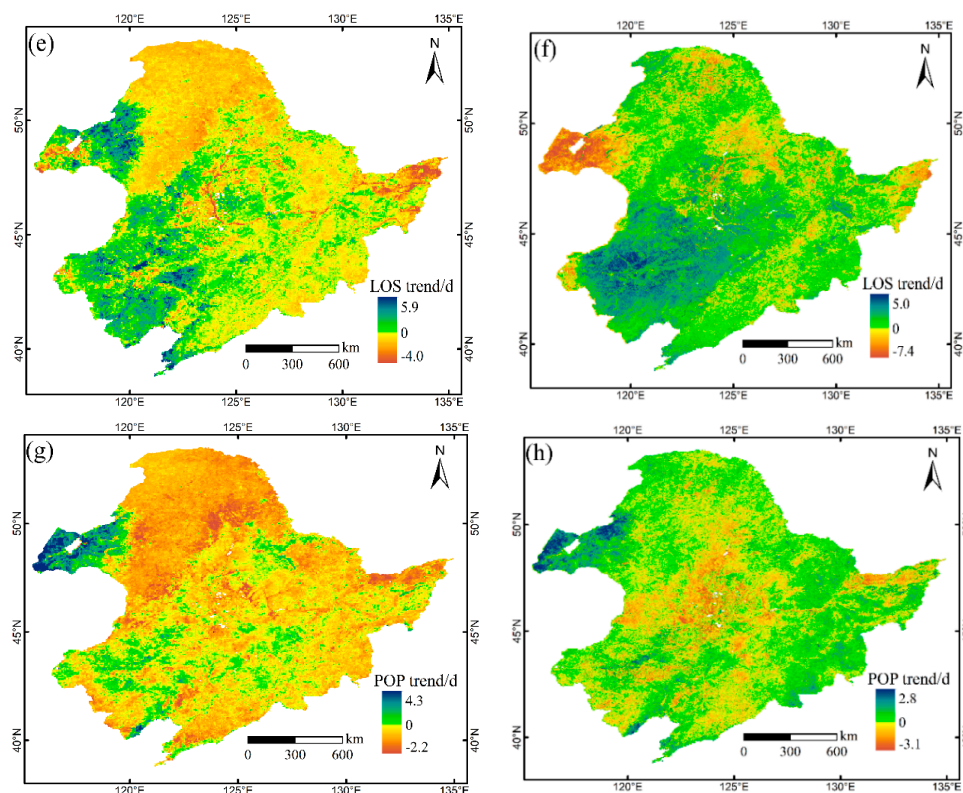


**Figure 5.** Spatial pattern of vegetation phenology trends in Northeastern China from 2001 to 2020. (a) SOS extracted by SIF (SOS<sub>SIF</sub>); (b) SOS extracted by NDVI (SOS<sub>NDVI</sub>); (c) EOS extracted by SIF (EOS<sub>SIF</sub>); (d) EOS extracted by NDVI (EOS<sub>NDVI</sub>); (e) LOS extracted by SIF (LOS<sub>SIF</sub>); (f) LOS extracted by NDVI (LOS<sub>NDVI</sub>); (g) POP extracted by SIF (POP<sub>SIF</sub>); (h) POP extracted by NDVI (POP<sub>NDVI</sub>).

### 3.3. Future Sustainability Analysis in Vegetation Phenology

The H values of vegetation phenology parameters in Northeastern China were estimated using SIF and NDVI products at the pixel scale from 2001 to 2020. (Figure 6). The H-mean of the SOS, EOS, and POP based on SIF and NDVI for the whole Northeastern area was in the range of 0.43–0.49, indicating weak anti-sustainability, accounting for 60.85%, 58.8%, and 59.3%. In contrast to the LOS<sub>NDVI</sub>, the average H of the LOS<sub>SIF</sub> was 0.45, which mainly showed weak anti-sustainability (61.3%), while the average H of the LOS<sub>NDVI</sub> was 0.51, mainly showing weak sustainability (49%).

To further reveal the future sustainability of vegetation phenology trends, we overlaid the trends with the sustainability outcomes (Figure 7). The results showed that the SOS<sub>SIF</sub> was mainly dominated by AT-WAS (52.6%) and AT-WS (20.4%). The SOS<sub>NDVI</sub> was mainly dominated by DT-WAS (48%) and DT-WS (43.03%). Most vegetation EOS<sub>SIF</sub> and EOS<sub>NDVI</sub> were dominated by DT-WAS, with 35.85% and 42.64%, respectively. Then, the EOS<sub>SIF</sub> was AT-WS with 20.4%, and the EOS<sub>NDVI</sub> was DT-WS with 30.49%. Most vegetation LOS<sub>SIF</sub> was dominated by DT-WAS (42.6%), while the LOS<sub>NDVI</sub> was dominated by AT-WAS (37.85%) and AT-WS (44.09%). The future trends of vegetation POP<sub>SIF</sub> and POP<sub>NDVI</sub> were consistent, dominated by AT-WAS (43.6%, 37.56%) and DT-WAS (16.5%, 23.88%).

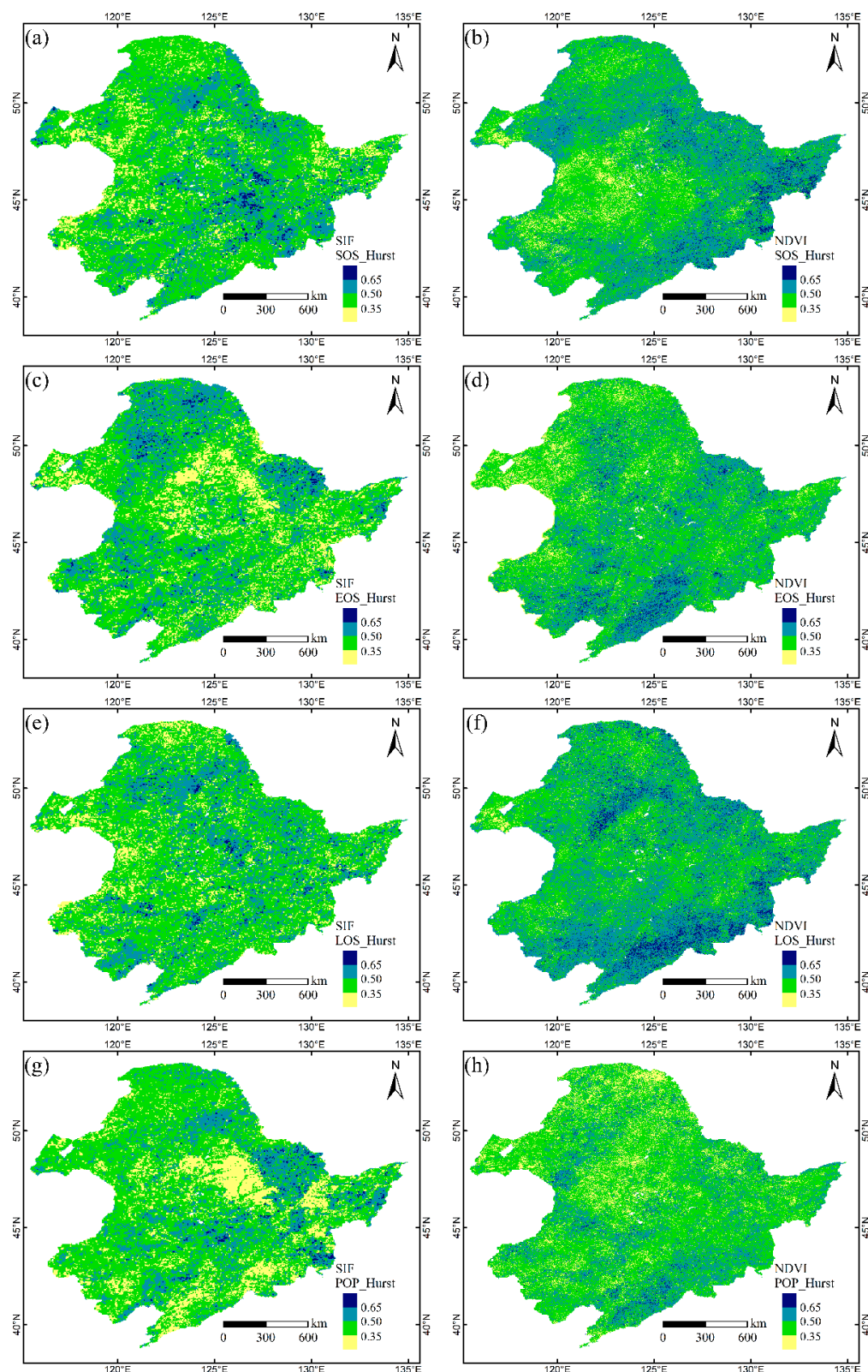


**Figure 6.** Spatial pattern of vegetation phenology parameter persistence in Northeastern China from 2001 to 2020. (a) SOS extracted by SIF ( $SOS_{SIF}$ ); (b) SOS extracted by NDVI ( $SOS_{NDVI}$ ); (c) EOS extracted by SIF ( $EOS_{SIF}$ ); (d) EOS extracted by NDVI ( $EOS_{NDVI}$ ); (e) LOS extracted by SIF ( $LOS_{SIF}$ ); (f) LOS extracted by NDVI ( $LOS_{NDVI}$ ); (g) POP extracted by SIF ( $POP_{SIF}$ ); (h) POP extracted by NDVI ( $POP_{NDVI}$ ).

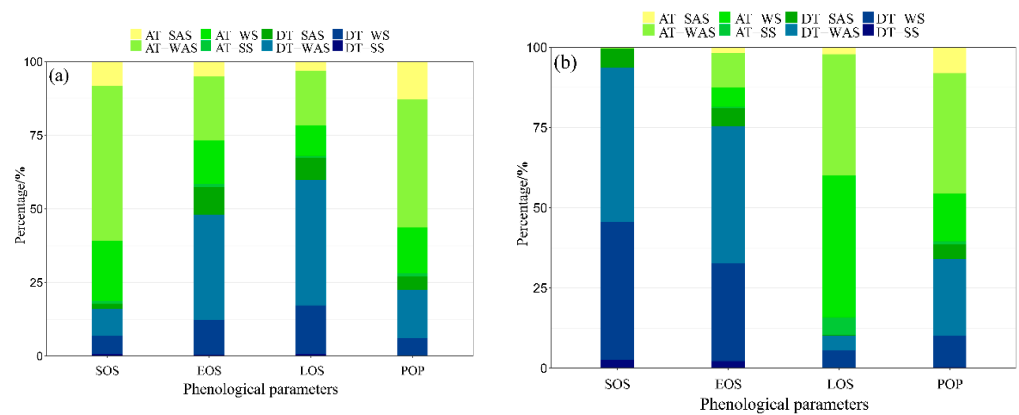


**Figure 7.** Proportion of future change trend of vegetation phenology in Northeastern China. **(a)** Proportion of future change trend of vegetation phenology based on SIF; **(b)** proportion of future change trend of vegetation phenology based on NDVI (advance-strong anti-sustainability: AT-SAS; advance-weak anti-sustainability: AT-WAS; advance-weak sustainability: AT-WS; advance-strong sustainability: AT-SAS; delayed-strong anti-sustainability: DT-SAS; delayed-weak anti-sustainability: DT-WAS; delayed-weak sustainability: DT-WS; delayed-strong sustainability: DT-SS).

### 3.4. Response of Phenology to Climate Change

We selected three climatic factors: temperature, precipitation, and relative humidity, to analyze the response mechanism of vegetation phenology (Figure 8). Temperature showed a slight upward trend, but the trend was not significant from 2001 to 2020 in Northeastern China. The increase in temperature was 1.02 °C in 20 years, with an average rate of 0.02 °C/year. Precipitation showed a clear upward trend up to about 163.88 mm, with an average rate of 5.08 mm/year. Relative humidity showed an obvious rising trend, with an increase of 6.67% in relative humidity over 20 years, at an average rate of 0.24%/year.

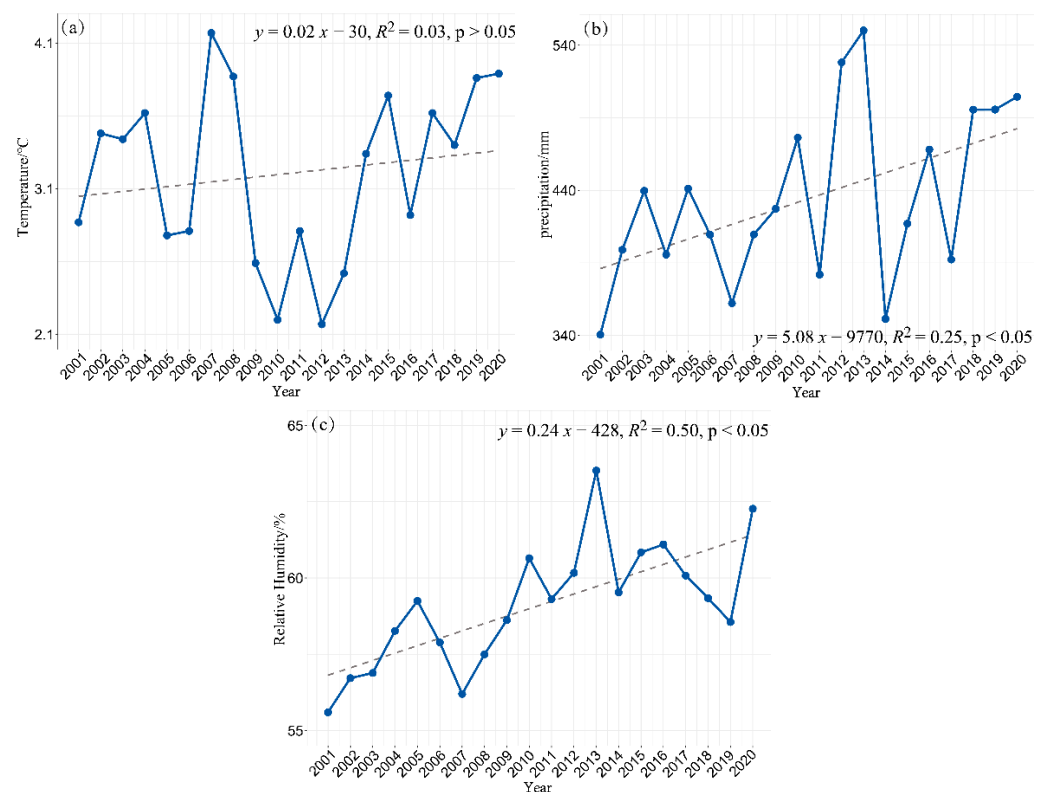


**Figure 8.** Interannual variation trend of Temp **(a)**, Prcp **(b)**, and RH **(c)** in Northeastern China.

### 3.4.1. Correlation between Climate Factors and Phenology of Different Vegetation Types

The correlation between climatic factors (Temp, Prcp, RH) and phenological parameters (SOS/EOS/LOS/POP) of different vegetation types based on two variables (SIF/NDVI) was analyzed (Figure 9). Temp was the most important factor affecting the SOS and LOS of GL, and the EOS and POP of SP. The SOS and LOS of SP, the LOS of SP, and the EOS and POP of GL all have the strongest response to Prcp. The effect of RH on the SOS of BF, the EOS and POP of CF, and the LOS of Mix B-C was most significant. There are significant differences in the correlation between different vegetation types and climate factors, including the  $EOS_{GL}$  and  $EOS_{SC}$ ,  $LOS_{SP}$ ,  $LOS_{CF}$ , and  $LOS_{BF}$  and  $LOS_{B-C}$ . The  $POP_{GL}$ ,  $POP_{SC}$ , and  $POP_{SP}$  were more consistent with climatic factors than the rest of the vegetation types. In particular, the correlations of the  $POP_{SIF}$  and  $POP_{NDVI}$  with meteorological factors were closer for SC than for other vegetation types.

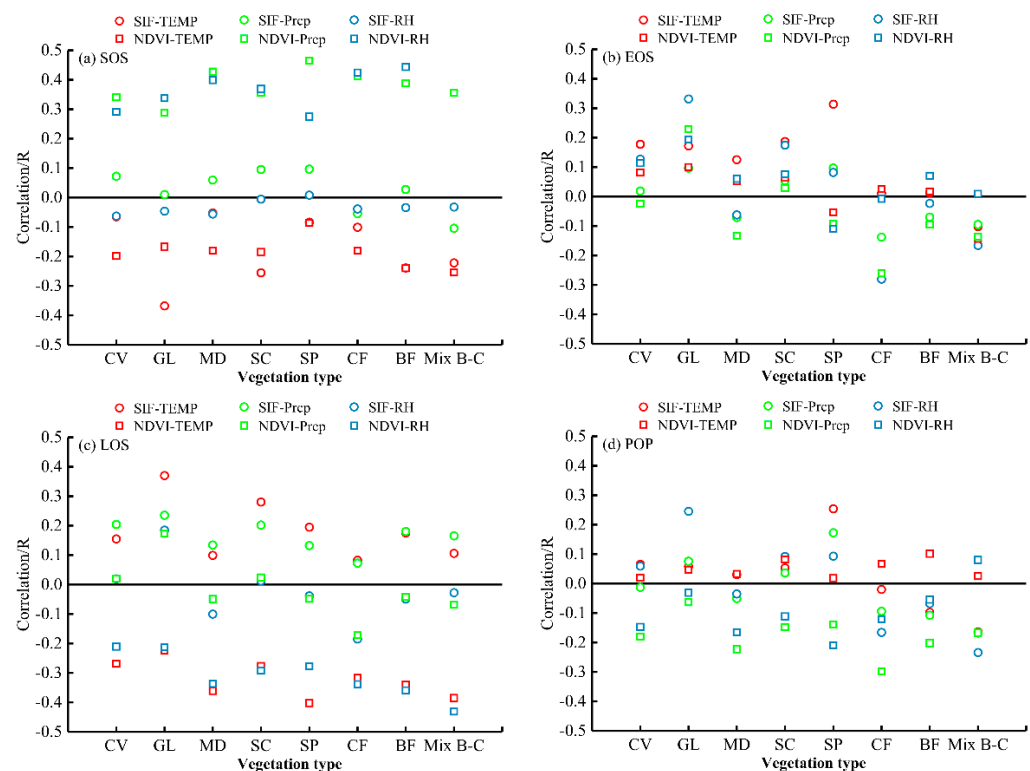


**Figure 9.** Correlation between phenology and climate factors of different vegetation types in North-eastern China from 2001 to 2020. (a) Correlation between SOS and climate factors based on SIF and NDVI; (b) correlation between EOS and climate factors based on SIF and NDVI; (c) correlation between LOS and climate factors based on SIF and NDVI; (d) correlation between POP and climate factors based on SIF and NDVI.

In general, the SOS was more sensitive to climate change than other phenological parameters. By comparing the results of SIF and MODIS, we found that the effect of Prcp and RH on the  $SOS_{NDVI}$  was much greater than that of the  $SOS_{SIF}$ , as well as the LOS by comparing the findings of SIF and MODIS. The  $EOS_{SIF}$  responded to the climate better. Temp and RH were more correlated with the  $POP_{SIF}$  than the  $POP_{NDVI}$ .

### 3.4.2. Response Analysis of Vegetation Phenology to Climate Factors at Different Scales

In order to more accurately analyze the response degree of vegetation phenology to Temp, Prcp, and RH, we correlated vegetation phenology with pre-season climate factors (Figure 10). The results showed that the correlation between the phenological parameters estimated by SIF and NDVI data and the pre-season climate was different. The  $SOS_{SIF}$  was mainly affected by the RH in March and April, and higher RH would lead to the advanced

SOS. The correlation between the  $SOS_{NDVI}$  and the pre-season climate was consistent, among which it was positively correlated with the Temp, and negatively correlated with Prcp and RH. The correlation between the  $EOS_{SIF}$  and Temp was the highest. The  $EOS_{NDVI}$  had a higher correlation with Prcp and RH, both of which were positively correlated. The  $LOS_{SIF}$  was mainly influenced by Prcp and RH. The  $LOS_{NDVI}$  was negatively correlated with Temp, but positively correlated with Prcp and RH. The  $POP_{SIF}$  and  $POP_{NDVI}$  had the same response to climate factors, mainly affected by Temp and RH, and the response mechanism was the opposite.

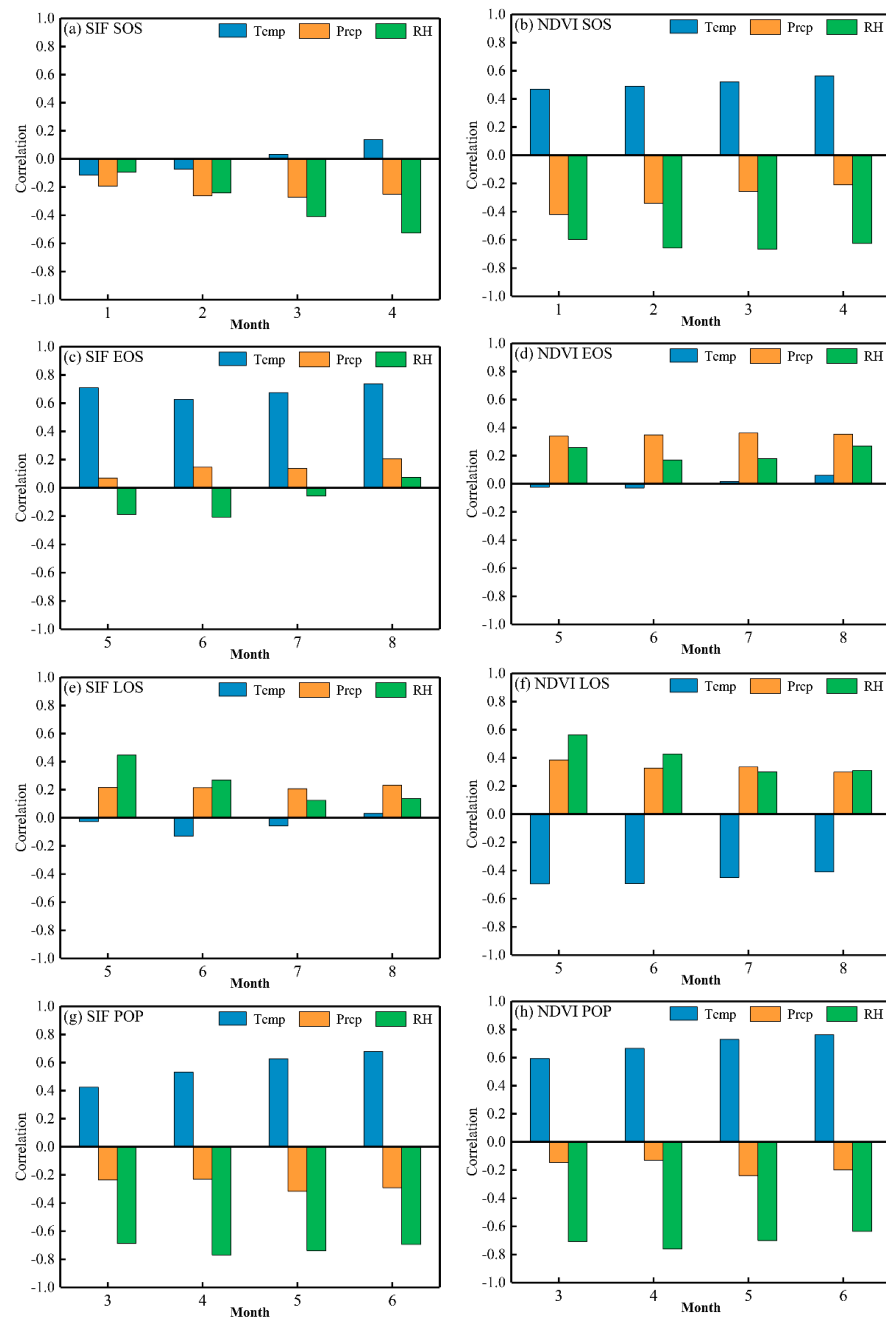


**Figure 10.** Correlation between vegetation phenological indicators and pre-seasonal climatic factors in Northeastern China. (a) Correlation between  $SOS_{SIF}$  and pre-season; (b) correlation between  $SOS_{NDVI}$  and pre-season; (c) correlation between  $EOS_{SIF}$  and pre-season; (d) correlation between  $EOS_{NDVI}$  and pre-season; (e) correlation between  $LOS_{SIF}$  and pre-season; (f) correlation between  $LOS_{NDVI}$  and pre-season; (g) correlation between  $POP_{SIF}$  and pre-season; (h) correlation between  $POP_{NDVI}$  and pre-season.

We investigated the spatial distribution of monthly climatic impacts on phenology at the pixel scale (Figure 11). We found that the vegetation  $SOS_{SIF}$  in the north and east was primarily influenced by February Temp and April Prcp, but the overall  $SIF_{NDVI}$  was most closely associated with March and April Temp, as well as Prcp in February, March, and April. The central plains and Hulunbuir grassland  $EOS_{SIF}$  was most strongly associated with July Temp and August Prcp, but the vegetation  $EOS_{NDVI}$  was primarily affected by August Temp, Prcp of May and June, and RH of June and August. The  $LOS_{SIF}$  was most strongly related to July Temp, May Prcp, and RH in the central plains and Hulunbuir grassland, while the  $LOS_{NDVI}$  was most strongly related to June and August Temp, except in northern Daxinganling, the Sanjiang plain, and the southern Changbai Mountain, where it was primarily affected by May Prcp and RH. The vegetation  $POP_{SIF}$  was influenced mostly by May Temp, Prcp of March and June, and RH of March and April. The  $POP_{NDVI}$  was influenced primarily by March and May temperature, March and June Prcp, and April and June RH.

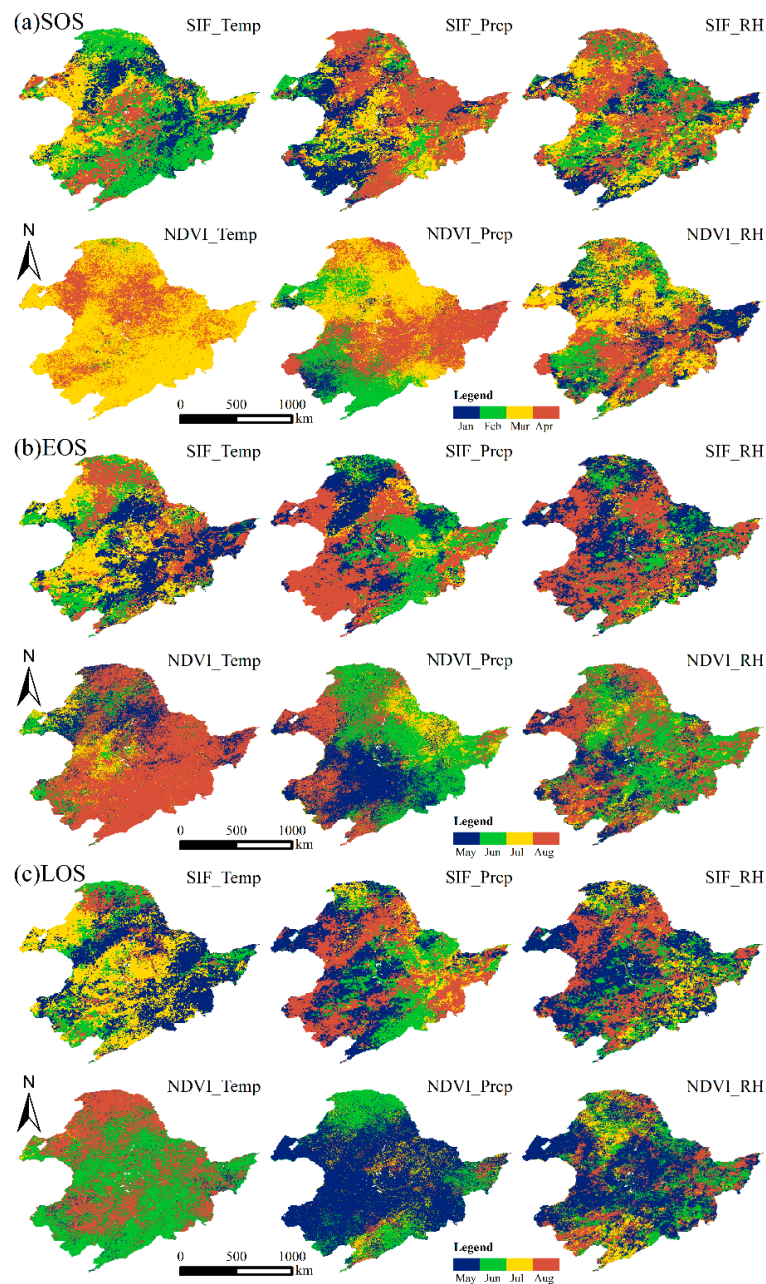
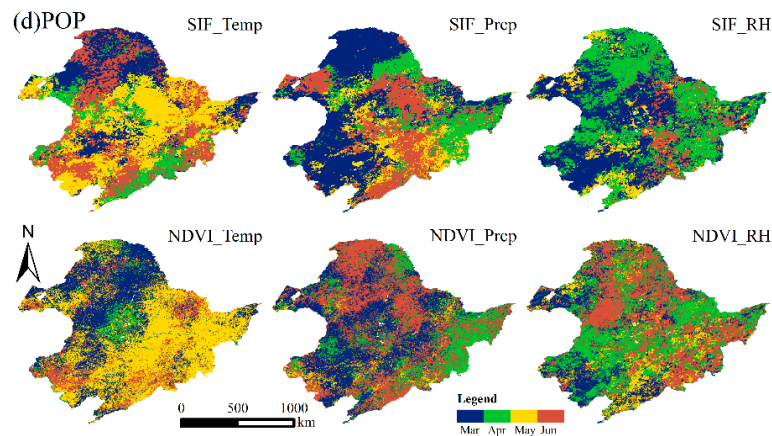


Figure 11. Cont.



**Figure 11.** The spatial distribution of the month with the maximum correlation between pre-season climate and phenological metrics in Northeastern China. (a) Month with maximum correlation between pre-season climate and SOS based on SIF and NDVI; (b) month with maximum correlation between pre-season climate and EOS based on SIF and NDVI; (c) month with maximum correlation between pre-season climate and LOS based on SIF and NDVI; (d) month with maximum correlation between pre-season climate and POP based on SIF and NDVI.

#### 4. Discussion

##### 4.1. Comparison of SIF and NDVI in Each Vegetation Type

The fitted curves of each vegetation type in Northeastern China were obtained by extracting the phenology curves of MODIS NDVI and SIF data (Figure 12). The results demonstrated that the NDVI and SIF curves in each vegetation type exhibited obvious variation characteristics with a complete single-peaked distribution, but there were some differences in the curve morphology, which resulted in significant variations in the phenological nodes that were produced. The NDVI time series curves of all vegetation types entered the spring onset early (except GL) and ended later. The peaks are gentler, especially in CF, BF, and Mix B-C, which have wider peaks, and the maximum values are relatively blurred. In contrast, the peaks of SIF time series curves were narrower in all vegetation types, and their growth peaks were more clearly defined. All of these resulted in longer and flatter  $LOS_{NDVI}$  than  $LOS_{SIF}$  for all vegetation types. This could be a result of the fact that SIF contains data on the stress states that are represented by both solar radiation and fluorescence efficiency. SIF data can successfully track variations in plant growth conditions over a large range induced by vegetation photosynthetic rate for the same vegetation index of greenness. As a result, SIF may be more sensitive to the inversion of vegetation phenology in Northeastern China.

##### 4.2. Interannual Variation of Phenological Parameters Based on SIF and NDVI

Vegetation phenology was estimated using SIF and NDVI products in Northeastern China, and interannual changes were compared (Figure 13). The results suggested that there were significant differences between the phenological dates estimated by SIF and MODIS NDVI. The  $SOS_{SIF}$  showed a weak advanced trend, and the  $SOS_{NDVI}$  showed a significant delayed trend. The  $EOS_{SIF}$  showed a delay over time, which was consistent with the  $EOS_{NDVI}$  trend, but the latter was more significant, and the EOS ended later. The changes in the SOS and EOS led to the prolongation of the  $LOS_{SIF}$  and the significant advance of the  $LOS_{NDVI}$ . However, the  $LOS_{SIF}$  was still shorter than the  $LOS_{NDVI}$ . Both the  $POP_{SIF}$  and the  $POP_{NDVI}$  had a downward trend, and the fluctuation state was first up and then down. The differences may be due to the large differences in seasonal cycles between leaf indices and photosynthesis [37]. Furthermore, the NDVI signal was easily affected by weather, such as clouds and snowfall, and the SIF signal was not affected by these factors [38], resulting in a large gap between the phenology estimated by SIF and NDVI.

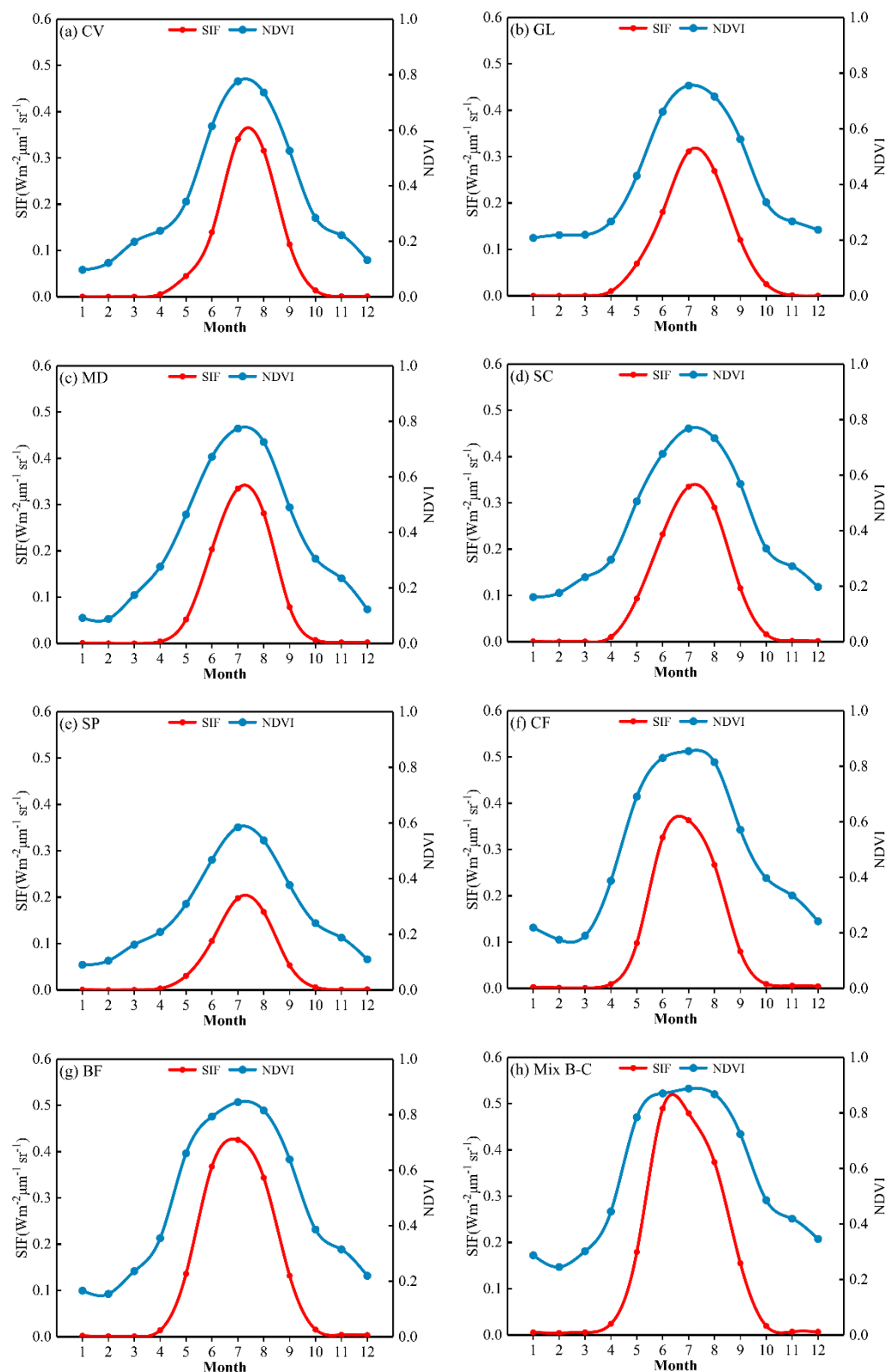


**Figure 12.** Time series of multi-year monthly mean for each vegetation type. (a) Time series of CV based on SIF and NDVI; (b) time series of GL based on SIF and NDVI; (c) time series of CV based on SIF and NDVI; (d) time series of CV based on SIF and NDVI; (e) time series of CV based on SIF and NDVI; (f) time series of CV based on SIF and NDVI; (g) time series of CV based on SIF and NDVI; (h) time series of CV based on SIF and NDVI.

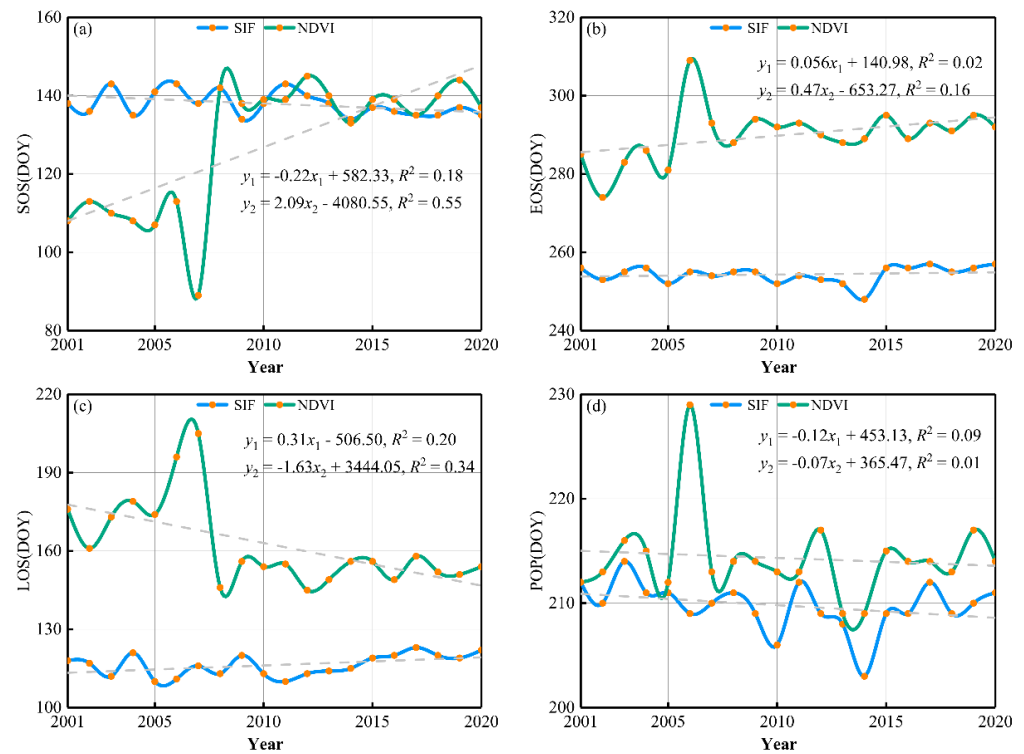


**Figure 13.** Interannual variation of vegetation phenological parameters deriving from SIF and NDVI time series in Northeastern China. (a) SOS extracted by SIF and NDVI; (b) EOS extracted by SIF and NDVI; (c) LOS extracted by SIF and NDVI; (d) POP extracted by SIF and NDVI.

Despite there being significant differences in time series between SIF and NDVI products, we also found some similarities in spatial patterns (Figure 3), which proved that SIF was reliable for monitoring vegetation phenology. Therefore, both SIF and NDVI products can be used to track temporal changes in vegetation phenology over the past decades.

#### 4.3. Environmental Response Mechanism of Vegetation Phenology

Air temperature is the basic requirement for vegetation growth and plays an important role in the development of vegetation. However, most of the vegetation energy is obtained through photosynthesis by sunlight [39]. Previous studies have also indicated the importance of solar radiation on phenology; that is, a longer photoperiod can extend the LOS of vegetation by prolonging the fall phenology and lengthening the growth season [40]. Vegetation needs sufficient cooling accumulation to enter the dormant winter phase and requires enough solar radiation to initiate vegetation growth, yet a warmer winter can cause vegetation to take longer for cooling accumulation, thus delaying phenological events [41–43]. Consequently, the effects of solar radiation on phenology should be considered when studying the environmental influence mechanisms of vegetation phenology.

#### 4.4. Uncertainty Analysis

There are uncertainties in the spatial resolution of SIF data to track vegetation phenology in Northeastern China, and the coarse spatial resolution of GOSIF data ( $0.05^\circ \times 0.05^\circ$ ) used in this paper has some limitations in tracking  $0.05^\circ \times 0.05^\circ$  phenology. However, it has been demonstrated that the GOSIF dataset has enormous potential for monitoring vegetation phenology and can assess the vegetation growth cycle more precisely than the traditional vegetation indices [44]. At the same time, GPP should be added as a covariate that may make the results more accurate and convincing.

## 5. Conclusions

Vegetation phenology has entered a stage of merging related disciplines and applying new approaches due to the growth of phenological observation techniques. We extracted vegetation phenology parameters from SIF and MODIS NDVI data in Northeastern China and compared spatial patterns and climatic response mechanisms to test the viability of SIF data in phenology estimation. The results showed that the greening stage of SIF started later (about 10 days), the yellowing stage ended earlier (about 36 days), and the growth peak of SIF was slightly earlier than NDVI. Although there are some differences in phenological dates between SIF and NDVI, their spatial distribution and future trend have some similarities. In addition, the vegetation phenology estimated by SIF was mainly controlled by temperature on the whole, while NDVI was mainly controlled by precipitation and relative humidity. Different phenological periods based on SIF and NDVI showed inconsistent responses to pre-season climate. SIF, as a novel remote sensing method, compensates for the shortcomings of classic vegetation indices in phenology extraction. Furthermore, this work may give scholarly references and proposals of major importance for the advancement of phenology and the understanding of ecological responses to global climate change.

**Author Contributions:** Conceptualization, R.Z., Y.Z. and T.H.; formal analysis, R.Z., Y.Z. and T.H.; funding acquisition, Y.Z. and T.H.; methodology, R.Z., Y.Z. and T.H.; data curation, W.S., S.Z., J.W. and H.W.; writing—original draft preparation, Y.Z. and T.H.; writing—review and editing, R.Z., Y.Z. and T.H. All authors have read and agreed to the published version of the manuscript.

**Funding:** This research was funded by the National Key Research and Development Program (Grant No. 2021xjkk0303).

**Institutional Review Board Statement:** Not applicable.

**Informed Consent Statement:** Not applicable.

**Data Availability Statement:** Not applicable.

**Conflicts of Interest:** The authors declare no conflict of interest.

## References

1. Zeng, L.; Wardlow, B.D.; Xiang, D.; Hu, S.; Li, D. A review of vegetation phenological metrics extraction using time-series, multispectral satellite data. *Remote Sens. Environ.* **2020**, *237*, 111511. [[CrossRef](#)]
2. Liu, Y.; Wang, J.; Dong, J.; Wang, S.; Ye, H. Variations of Vegetation Phenology Extracted from Remote Sensing Data over the Tibetan Plateau Hinterland during 2000–2014. *J. Meteorol. Res.-Prc.* **2020**, *34*, 786–797. [[CrossRef](#)]
3. Xie, Q.; Huete, A.; Hall, C.C.; Medlyn, B.E.; Power, S.A.; Davies, J.M.; Medek, D.E.; Beggs, P.J. Satellite-observed shifts in C3/C4 abundance in Australian grasslands are associated with rainfall patterns. *Remote Sens. Environ.* **2022**, *273*, 112983. [[CrossRef](#)]
4. Walther, G.R.; Post, E.; Convey, P.; Menzel, A.; Parmesan, C.; Beebee, T.J.; Fromentin, J.M.; Hoegh-Guldberg, O.; Bairlein, F. Ecological responses to recent climate change. *Nature* **2002**, *416*, 389–395. [[CrossRef](#)]
5. Tucker, C.J. Red and photographic infrared linear combinations for monitoring vegetation. *Remote Sens. Environ.* **1979**, *8*, 127–150. [[CrossRef](#)]
6. Huete, A.; Didan, K.; Miura, T.; Rodriguez, E.P.; Gao, X.; Ferreira, L.G. Overview of the radiometric and biophysical performance of the MODIS vegetation indices. *Remote Sens. Environ.* **2002**, *83*, 195–213. [[CrossRef](#)]
7. Hmimina, G.; Dufrêne, E.; Pontailier, J.Y.; Delpierre, N.; Aubinet, M.; Caquet, B.; de Grandcourt, A.; Burban, B.; Flechard, C.; Granier, A.; et al. Evaluation of the potential of MODIS satellite data to predict vegetation phenology in different biomes: An investigation using ground-based NDVI measurements. *Remote Sens. Environ.* **2013**, *132*, 145–158. [[CrossRef](#)]
8. Melaas, E.K.; Friedl, M.A.; Zhu, Z. Detecting interannual variation in deciduous broadleaf forest phenology using Landsat TM/ETM+ data. *Remote Sens. Environ.* **2013**, *132*, 176–185. [[CrossRef](#)]
9. Lu, X.; Cheng, X.; Li, X.; Chen, J.; Sun, M.; Ji, M.; He, H.; Wang, S.; Li, S.; Tang, J. Seasonal patterns of canopy photosynthesis captured by remotely sensed sun-induced fluorescence and vegetation indexes in mid-to-high latitude forests: A cross-platform comparison. *Sci. Total Environ.* **2018**, *644*, 439–451. [[CrossRef](#)]
10. Wu, C.; Gonsamo, A.; Gough, C.M.; Chen, J.M.; Xu, S. Modeling growing season phenology in North American forests using seasonal mean vegetation indices from MODIS. *Remote Sens. Environ.* **2014**, *147*, 79–88. [[CrossRef](#)]
11. Wong, C.Y.; Gamon, J.A. The photochemical reflectance index provides an optical indicator of spring photosynthetic activation in evergreen conifers. *New Phytol.* **2015**, *206*, 196–208. [[CrossRef](#)] [[PubMed](#)]

12. Richardson, A.D.; Braswell, B.H.; Hollinger, D.Y.; Jenkins, J.P.; Ollinger, S.V. Near-surface remote sensing of spatial and temporal variation in canopy phenology. *Ecol. Appl.* **2009**, *19*, 1417–1428. [[CrossRef](#)] [[PubMed](#)]
13. Richardson, A.D.; Andy Black, T.; Ciais, P.; Delbart, N.; Friedl, M.A.; Gobron, N.; Hollinger, D.Y.; Kutsch, W.L.; Longdoz, B.; Luyssaert, S.; et al. Influence of spring and autumn phenological transitions on forest ecosystem productivity. *Philos. Trans. R. Soc. Lond. Ser. B Biol. Sci.* **2010**, *365*, 3227–3246. [[CrossRef](#)] [[PubMed](#)]
14. Sophia, W.; Maximilian, V.; Tea, T.; Alemu, G.; Yongguang, Z.; Philipp, K.; Martin, J.; Andrej, V.; Luis, G. Satellite chlorophyll fluorescence measurements reveal large-scale decoupling of photosynthesis and greenness dynamics in boreal evergreen forests. *Glob. Chang. Biol.* **2016**, *22*, 2979–2996.
15. Joiner, J.; Yoshida, Y.; Vasilkov, A.P.; Yoshida, Y.; Corp, L.A. First observations of global and seasonal terrestrial chlorophyll fluorescence from space. *Biogeosciences* **2011**, *8*, 637–651. [[CrossRef](#)]
16. Wang, X.; Dannenberg, M.P.; Yan, D.; Jones, M.O.; Kimball, J.S.; Moore, D.; Leeuwen, W.; Didan, K.; Smith, W.K. Globally Consistent Patterns of Asynchrony in Vegetation Phenology Derived From Optical, Microwave, and Fluorescence Satellite Data. *J. Geophys. Res. Biogeosci.* **2020**, *125*, e2020JG005732. [[CrossRef](#)]
17. Guo, M.; Li, J.; Huang, S.; Wen, L. Feasibility of Using MODIS Products to Simulate Sun-Induced Chlorophyll Fluorescence (SIF) in Boreal Forests. *Remote Sens.* **2020**, *12*, 680. [[CrossRef](#)]
18. Mao, D.-H.; Wang, Z.-M.; Luo, L.; Han, J.-X. Dynamic changes of vegetation net primary productivity in permafrost zone of Northeast China in 1982–2009 in response to global change. *Ying Yong Sheng Tai Xue Bao = J. Appl. Ecol.* **2012**, *23*, 1511–1519.
19. Yanjun, S.; Qinghua, G.; Tianyu, H.; Hongcan, G.; Shichao, J.; Shazhou, A.; Xuelin, C.; Ke, G.; Zhanqing, H.; Yuanman, H.; et al. An updated Vegetation Map of China (1:1000000). *Sci. Bull.* **2020**, *65*, 1125–1136.
20. Li, X.; Xiao, J. A Global, 0.05-Degree Product of Solar-Induced Chlorophyll Fluorescence Derived from OCO-2, MODIS, and Reanalysis Data. *Remote Sens.* **2019**, *11*, 517. [[CrossRef](#)]
21. Gao, K.; Xu, J.; Gao, G.; Li, Y.; Hutchins, D.A.; Huang, B.; Wang, L.; Zheng, Y.; Jin, P.; Cai, X.; et al. Rising CO<sub>2</sub> and increased light exposure synergistically reduce marine primary productivity. *Nat. Clim. Chang.* **2012**, *2*, 519–523. [[CrossRef](#)]
22. Xiao, J.; Zhuang, Q.; Baldocchi, D.D.; Law, B.E.; Richardson, A.D.; Chen, J.; Oren, R.; Starr, G.; Noormets, A.; Ma, S.; et al. Estimation of net ecosystem carbon exchange for the conterminous United States by combining MODIS and AmeriFlux data. *Agric. For. Meteorol.* **2008**, *148*, 1827–1847. [[CrossRef](#)]
23. Peng, S.; Gang, C.; Cao, Y.; Chen, Y. Assessment of climate change trends over the Loess Plateau in China from 1901 to 2100. *Int. J. Climatol.* **2018**, *38*, 2250–2264. [[CrossRef](#)]
24. Peng, S.; Ding, Y.; Liu, W.; Zhi, L.I. 1 km monthly temperature and precipitation dataset for China from 1901 to 2017. *Earth Syst. Sci. Data* **2019**, *11*, 1931–1946. [[CrossRef](#)]
25. Peng, S.; Ding, Y.; Wen, Z.; Chen, Y.; Cao, Y.; Ren, J. Spatiotemporal change and trend analysis of potential evapotranspiration over the Loess Plateau of China during 2011–2100. *Agric. For. Meteorol.* **2017**, *233*, 183–194. [[CrossRef](#)]
26. Ding, D.; Peng, S. Spatiotemporal Trends and Attribution of Drought across China from 1901–2100. *Sustainability* **2020**, *12*, 477. [[CrossRef](#)]
27. Li, X.; Zhou, Y.; Asrar, G.R.; Meng, L. Characterizing spatiotemporal dynamics in phenology of urban ecosystems based on Landsat data. *Sci. Total Environ.* **2017**, *605–606*, 721–734. [[CrossRef](#)]
28. Guan, K.; Wood, E.F.; Medvigy, D.; Kimball, J.; Pan, M.; Caylor, K.K.; Sheffield, J.; Xu, X.; Jones, M.O. Terrestrial hydrological controls on land surface phenology of African savannas and woodlands. *J. Geophys. Res. Biogeosci.* **2014**, *119*, 1652–1669. [[CrossRef](#)]
29. Shang, R.; Liu, R.; Xu, M.; Liu, Y.; Zuo, L.; Ge, Q. The relationship between threshold-based and inflexion-based approaches for extraction of land surface phenology. *Remote Sens. Environ.* **2017**, *199*, 167–170. [[CrossRef](#)]
30. Ma, X.; Huete, A.; Moran, S.; Campos, G.P.; Eamus, D. Abrupt shifts in phenology and vegetation productivity under climate extremes. *J. Geophys. Res. Biogeosci.* **2015**, *120*, 2036–2052. [[CrossRef](#)]
31. Li, G.; Li, X.; Zhao, G.; Zhang, Z.; Li, Y. Characteristics of spatial and temporal phenology under the dynamic variation of grassland in the Qinghai Lake watershed. *Acta Ecol. Sin.* **2014**, *34*, 3038–3047.
32. Hurst, H.E. Long-Term Storage Capacity of Reservoirs. *Trans. Am. Soc. Civ. Eng.* **1951**, *116*, 770–799. [[CrossRef](#)]
33. Li, S.; Yan, J.; Liu, X.; Wan, J. Response of vegetation restoration to climate change and human activities in Shaanxi-Gansu-Ningxia Region. *J. Geogr. Sci.* **2013**, *23*, 98–112. [[CrossRef](#)]
34. Miao, L.; Jiang, C.; Xue, B.; Liu, Q.; He, B.; Nath, R.; Cui, X. Vegetation dynamics and factor analysis in arid and semi-arid Inner Mongolia. *Environ. Earth Sci.* **2015**, *73*, 2343–2352. [[CrossRef](#)]
35. Seddon, A.; Macias-Fauria, M.; Long, P.R.; Benz, D.; Willis, K.J. Sensitivity of global terrestrial ecosystems to climate variability. *Nature* **2016**, *531*, 229–232. [[CrossRef](#)] [[PubMed](#)]
36. Tong, X.; Wang, K.; Brandt, M.; Yue, Y.; Liao, C.; Fensholt, R. Assessing Future Vegetation Trends and Restoration Prospects in the Karst Regions of Southwest China. *Remote Sens.* **2016**, *8*, 357. [[CrossRef](#)]
37. Zhang, Y.; Commene, R.; Zhou, S.; Williams, A.P.; Gentine, P. Light limitation regulates the response of autumn terrestrial carbon uptake to warming. *Nat. Clim. Chang.* **2020**, *10*, 739–743. [[CrossRef](#)]
38. Zhang, Y.; Joiner, J.; Alemohammad, S.H.; Zhou, S.; Gentine, P. A global spatially contiguous solar-induced fluorescence (CSIF) dataset using neural networks. *Biogeosciences* **2018**, *15*, 5779–5800. [[CrossRef](#)]

39. Xie, Y.; Wang, X.; Silander, J.A., Jr. Deciduous forest responses to temperature, precipitation, and drought imply complex climate change impacts. *Proc. Natl. Acad. Sci. USA* **2015**, *112*, 13585–13590. [[CrossRef](#)]
40. Liu, L.; Zhang, X. Effects of temperature variability and extremes on spring phenology across the contiguous United States from 1982 to 2016. *Sci. Rep.* **2020**, *10*, 17952. [[CrossRef](#)]
41. Yu, L.; Han, Y.; Jiang, Y.; Dong, T.; Lei, Y. Sex-specific responses of bud burst and early development to nongrowing season warming and drought in *Populus cathayana*. *Can. J. Forest Res.* **2017**, *48*, 68–76. [[CrossRef](#)]
42. Signarbieux, C.; Toledano, E.; Sangines de Carcer, P.; Fu, Y.H.; Schlaepfer, R.; Buttler, A.; Vitasse, Y. Asymmetric effects of cooler and warmer winters on beech phenology last beyond spring. *Glob. Chang. Biol.* **2017**, *23*, 4569–4580. [[CrossRef](#)]
43. Schieber, B.; Kubov, M.; Jank, R. Effects of Climate Warming on Vegetative Phenology of the Common Beech *Fagus sylvatica* in a Submontane Forest of the Western Carpathians: Two-Decade Analysis. *Pol. J. Ecol.* **2017**, *65*, 339–351.
44. Qiu, R.; Li, X.; Han, G.; Xiao, J.; Ma, X.; Gong, W. Monitoring drought impacts on crop productivity of the U.S. Midwest with solar-induced fluorescence: GOSIF outperforms GOME-2 SIF and MODIS NDVI, EVI, and NIRv. *Agric. For. Meteorol.* **2022**, *323*, 109038. [[CrossRef](#)]

**Disclaimer/Publisher’s Note:** The statements, opinions and data contained in all publications are solely those of the individual author(s) and contributor(s) and not of MDPI and/or the editor(s). MDPI and/or the editor(s) disclaim responsibility for any injury to people or property resulting from any ideas, methods, instructions or products referred to in the content.